Electrochemical Corrosion Performance of Aromatic Functionalized Imidazole Inhibitor Under Hydrodynamic Conditions on API X65 Carbon Steel in 1 M HCl Solution

A. Ismail[1] · H. M. Irshad[2] · A. Zeino[1] · I. H. Toor[2,3]

Abstract

The hydrodynamic corrosion inhibitive performance of two imidazole derivatives 2-ethyl-4-methylimidazole and 1-benzylimidazole was investigated on API X65 steel in 1.0 M HCl solution. Structural features of the molecules derived from density functional theory (DFT) calculations at B3LYP/6-31G(d.p) showed that 1-benzylimidazole possess high electron density due to π network which lies flat on the surface and tends to form a stronger interaction with the metal. The addition of the inhibitor molecules in 1 M HCl solution shifted the corrosion potential (E_{corr}) in the noble direction. Tafel polarization and electrochemical impedance spectroscopy (EIS) experiments performed at 0–1500 rpm and 50–500 ppm of inhibitor concentration revealed that the corrosion rate was increased with an increase in rotation speed in the absence of inhibitor molecules. However, upon the addition of the inhibitor molecules in the solution minimized the corrosion rate with an efficiency of 82% in the case of 1-benzylimidazole at 500 ppm and 500 rpm electrode rotation. It was concluded that simple imidazole molecules could serve as corrosion inhibitors under extreme hydrodynamic conditions.

Keywords Imidazole · API X65 steel · Rotating disk electrode (RDE) · DFT · Hydrodynamic

1 Introduction

Metallic structures deteriorate progressively by an electrochemical process of corrosion. The process industries, transportation pipelines and fluid handling equipment damaged severely because of corrosion process, and this contributed toward huge economic loss in terms of increased maintenance/repair, replacement and inspection/monitoring of damaged pipelines. Therefore, to reduce loss and to enhance reliability of metallic structures, suitable corrosion protection strategies must be employed and one of such strategies is to use compatible chemical inhibitors in aggressive fluids [1–3] Inhibitors are commonly used in petrochemical and process industries for protection and chemical cleaning during production [4]. The cutting tools and cooling systems mostly face high temperatures and turbulent flow in severe conditions, and this reduces the lifetime of cutting tools. It has been reported that the addition of inhibitors under such situations increased the life of cutting tools [5–8].

The corrosion rate of bare materials depends on many factors such as the characteristics of a metallic material, aggressiveness of the solution in terms of its concentration of chemical species and temperature. The structure and chemical composition of the inhibitor interacting with the metal surface will determine its inhibition efficiency in decreasing the corrosion rate in that environment. Acid solutions are used for acid cleaning, oil well acidizing, descaling and acid pickling in different process industries. Different inhibitors are being used to protect the infrastructure in acid solutions [9–14], and most of these organic inhibitors contain nitrogen, oxygen, sulfur and aromatic ring [15,16]. Corrosion inhibition performance of an inhibitor is related to its molecular structure and that depends on various parameters, such as electronic distribution, type of functional group, aromaticity and frontier molecular orbitals (HOMO and LUMO).

✉ I. H. Toor
ihsan@kfupm.edu.sa; toorihsan@gmail.com

1 Chemistry Department, King Fahd University of Petroleum and Minerals, Dhahran 31261, Kingdom of Saudi Arabia

2 Mechanical Engineering Department, King Fahd University of Petroleum and Minerals, Dhahran 31261, Kingdom of Saudi Arabia

3 Center of Research Excellence in Nanotechnology, King Fahd University of Petroleum & Minerals (KFUPM), Dhahran 31261, Kingdom of Saudi Arabia

Structural features such as electron affinity (A), global hardness (η), electronegativity (χ), ionization potential (I) and dipole moment (μ) also play a key role in determining the inhibition efficiency. These features calculated using density functional theory (DFT), a computational quantum mechanical modeling method, provide a predictive insight into the corrosion inhibitive characteristics of inhibitor molecules [17]. Over the years, DFT has grown to be an efficient theoretical method, which can investigate the interaction between the metallic surface and the inhibitor and structural nature of inhibitor, and can interpret the experimental behavior. There have been recent investigations on the use of benzimidazole compounds in petroleum industry to examine their effectiveness in cleaning of boilers and heat exchangers in acid media and results were found very promising [18]. A rotating disk electrode (RDE) experimental setup was used to evaluate the behavior of various corrosion inhibitors for the petroleum industry in order to predict the corrosion rate of pipe wall efficiently. RDE is fixed in an insulating sheath of larger diameter and a disk specimen inside can be exposed to the solution under dynamic conditions. It is rotated about an axis, which is normal to the surface of the disk electrode. This acts as a pump which pulls the solution upward and then throw outwards [19]. Such a setup can be used to investigate the general corrosion rate economically and rapidly with a uniformly accessible surface [20–23]. There are many reports on the effect of corrosion inhibitors in the petrochemical industry under static conditions; however, the data under dynamic condition are rarely reported. So, the aim of this study was to evaluate the anti-corrosion behaviors of 2-ethyl-4-methylimidazole and 1-benzylimidazole inhibitors under dynamic conditions. The efficiency of these compounds as corrosion inhibitors for API X65 steel in 1.0 M HCl was investigated by electrochemical techniques using a three-electrode cell in RDE system.

2 Experimental

2.1 Computational Procedure

DFT calculations were carried out using the Gaussian 09 package [24], with hybrid function of the Becke three-parameter Lee, Yang and Par (B3LYP) method and 6-31G(d.p) basis set. Aqueous-phase calculations were carried out using SMD implicit solvation model implemented on GaussView 5.0 [25]. Structural geometry of each molecule was optimized, and the vibrational frequency analysis showed no imaginary frequency prior to the computational calculations. Structural parameters such as global hardness (η), electron affinity (A), ionization potential (I), electronegativity (χ) and dipole moment (μ) were subsequently calculated.

According to DFT Koopman's theorem [26], the ionization potential I can be approximated as the negative of the highest occupied molecular orbital (HOMO) energy,

$$I = -E_{\text{HOMO}} \tag{1}$$

Electron affinity A is approximated in the same manner as the negative of the lowest unoccupied molecular orbital (LUMO) energy,

$$A = -E_{\text{LUMO}} \tag{2}$$

Electronegativity χ is defined as,

$$\chi = -\mu = \frac{I + A}{2} \tag{3}$$

Global hardness η is calculated as follows,

$$\eta = \frac{I - A}{2} \tag{4}$$

while global softness σ is the inverse of global hardness

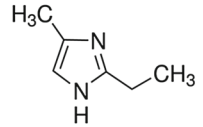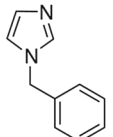$$\sigma = \frac{1}{\eta} \tag{5}$$

2.2 Reagents and Solutions

The analytical-grade reagents (2-ethyl-4-methylimidazole and 1-benzylimidazole) from Sigma-Aldrich were of standard purity and used as-received without further purifications. The solutions were prepared by dissolving the appropriate masses in 1.0 M HCl (Fluka) using double-distilled water. The structures of the molecules, their abbreviations and their respective molar masses are given in Table 1.

2.3 Electrochemical Studies

Corrosion tests were carried out using a Gamry rotating disk electrode (RDE 710) equipped with a three-electrode cell opened to the air, which composed of a specimen as a working electrode, a Pt wire as a counter electrode and a saturated calomel reference electrode (SCE). API X65 (C, 0.04–0.16%; Mn, 1.00–1.60%; P, 0.02%; S, 0.01%; Si, 0.45%; V, 0.09%; Nb, 0.05%; Ti, 0.06%, remaining Fe) was used as a working electrode in these investigations. The specimens were ground with emery paper up to 800 grits, degreased with acetone and cleaned ultrasonically in distilled water prior to electrochemical tests. The electrochemical investigations were carried out with an exposed working electrode area of $0.2 \, \text{cm}^2$ in chloride solution at room temperature in Gamry potentiostat (Reference 3000) and repeated thrice to ensure the reproducibility of

Table 1 Inhibitor molecules under study

Inhibitor	Structure	Abbreviation	Molecular weight (g/mol)
2-Ethyl-4-methylimidazole		2-EM-Imz	110.16
1-Benzylimidazole		1-B-Imz	158.20

the data. DC105 corrosion software was used to conduct Tafel polarization experiments as well as electrochemical impedance spectroscopy. Tafel curves were obtained by scanning the potential at 1.0 mV/s in the range $+250$ mV to -250 mV against the open-circuit potential (E_{ocp}). Corrosion potential ($E_{corr} V_{SCE}$) and corrosion current density (i_{corr}, A cm^{-2}) were obtained by extrapolation of anodic (β_a) and cathodic (β_c) branches of the Tafel curves. Electrochemical impedance spectroscopy measurements (EIS) were taken at open-circuit potential (E_{ocp} vs SCE) in the frequency range 100 KHz to 100 mHz, with amplitude of perturbation 10 mV r.m.s. Gamry Echem Analyst version 6.03 was used for data analysis and fittings. Open-circuit potential measurements of the inhibitor molecules were taken during two hours of immersion in 50 ppm freshly prepared solutions in 1.0 M HCl. To determine whether the flow of the medium was laminar or turbulent, the Reynolds numbers were calculated.

3 Results and Discussion

3.1 Computational Studies

Structural properties of the molecules under study derived from DFT calculations using the B3LYP method and 6-31G(d.p) basis set are summarized in Table 2. The table shows the gas-phase optimized structural geometries, the frontier orbital diagrams (HOMO, LUMO) and the molecular electrostatic potential (MEP) maps of the inhibitor molecules, respectively. The tendency of an inhibitor molecule to adsorb on metallic surfaces has been linked to the donor–acceptor interaction indices of the molecule obtained from DFT studies [27–30]. The HOMO electron density distribution serves as the region of the molecule from where electrons are readily donated to the vacant orbitals of metal. The LUMO electron density distribution on the other hand

reveals the molecular centers that are prone to electron back-acceptance from the occupied d orbitals of the metal [31].

Examining the HOMO electron distribution of the molecules revealed that the electron density is distributed over the nitrogen heteroatoms of the imidazole ring. This indicates that the molecules can interact with the metal atoms by donating charges from the electron-rich centers to the vacant d orbitals of the metal atom. The corresponding LUMO electron density distribution of the molecules indicates that the molecules are capable of accepting charges using the electron density-deficient centers, which shows their ability to form a strong interaction with the metal. Similarly, the molecular electrostatic potential maps of the molecules as given in Table 2 indicate the region of high electron density on the molecules, with the regions in red signifying electron-rich sites and those in blue electron-deficient sites. This explains the HOMO–LUMO electron density distribution already discussed. The overall chemical reactivity indicators and quantum chemical descriptors of the molecules derived from DFT calculations in both gaseous and aqueous phases are summarized in Table 3.

Parameters which include the HOMO energy (E_{HOMO}), LUMO energy (E_{LUMO}), HOMO–LUMO energy gap (ΔE), global hardness (η), global softness (σ) and electronegativity (χ) are listed in Table 3. It has been established that a high value of E_{HOMO}, and/or low value of E_{LUMO}, a small ΔE, a low value of η, and/or a high value of χ is an indication of a better inhibition performance of a molecule. Global hardness (η), a measure of chemical reactivity of a molecule, indicates the resistance of a molecule to electron density distortion. Molecules with high global hardness are usually less reactive and tend to adsorb less on the metal according to the hard–soft acid base (HSAB) theory [32]. Molecules with high global softness on the other hand are easily polarized and prone to acquire electronic charge. This in turn enhances their ability to adsorb on the metal surface, acting as corro-

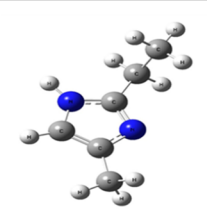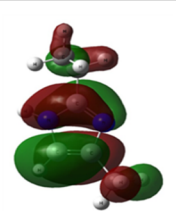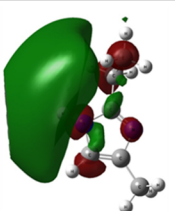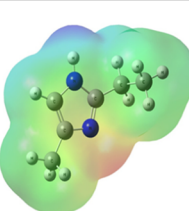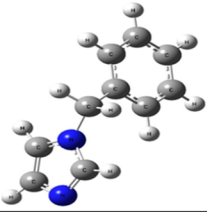**Table 2** Structural features of inhibitor molecules obtained at B3LYP/6-31G(d.p)
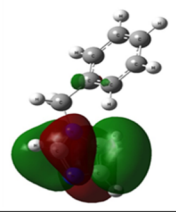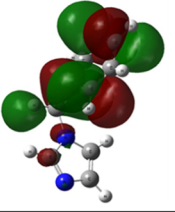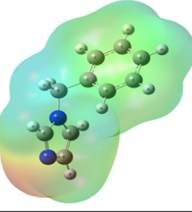
Molecule	Optimized geometry	HOMO diagram	LUMO diagram	MEP map
2-EM-Imz				
1-B-Imz				

Table 3 Structural data of inhibitor molecules obtained at B3LYP/6-31G(d.p)

Molecule	Phase	E_{HOMO} (eV)	E_{LUMO} (eV)	$\Delta E_{\text{L–H}}$ (eV)	η (eV)	χ (eV)	σ (eV^{-1})
2-EM-Imz	Gas	-5.975	-0.487	5.488	2.744	3.231	0.364
	Water	-6.015	-0.098	5.917	2.959	3.057	0.338
1-B-Imz	Gas	-6.431	-0.893	5.538	2.769	3.662	0.361
	Water	-6.439	-0.668	5.771	2.886	3.552	0.346

sion inhibitors. From Table 3, 2-EM-Imz was found to have a lower HOMO–LUMO energy gap (ΔE) and tend to be softer in the gaseous phase. Hence, it would be projected to have a better interaction with the metal. However, the electronegativity (χ) results showed that 1-B-Imz has a high electron cloud due to the presence of the phenyl ring in the molecule and this tends to furnish the metal with electrons forming a stronger interaction. Since several factors contribute to the inhibition performance of a given molecule, we further carried out experimental studies to investigate the inhibition performance of the molecules.

3.2 Open-Circuit Potential

Prior to electrochemical test, open-circuit potential (OCP) was measured in 1.0 M HCl in the absence (blank) and presence of 50 ppm inhibitor molecules under dynamic conditions to optimize the immersion time before each experiment. The results of Fig. 1 showed a corresponding shift in noble direction when the inhibitor molecules were used as compared to the blank medium. It is clear that open-circuit potential became almost completely stable after about 60 min of immersion time, which is an indication of attainment of steady state. The open-circuit potential trend followed the order, i.e., 1-B-Imz > 2-EM-Imz > blank solution, which

implies a possible increase in the inhibition efficiency of the molecules in that order. It is reported that the inhibitive properties of any molecule are linked to its OCP value, i.e., a molecule with a lower (more negative) potential is considered less efficient compared to that with a higher (more positive) potential. Since there was no significant difference in OCP values after 60 min of immersion, new OCP values were measured after 120 min of immersion.

OCP is a mixed potential that results from the kinetics of the dominant anodic and cathodic processes in an electrochemical reaction. It is can be used to study the performance of corrosion inhibitors on the metal surface under open-circuit conditions (without the application of external current). It gives the potential at which the metal will corrode or passivate without the application of external current. Choudhary et al. [33] studied the relationship between OCP and polarization resistance of mild steel in 3.5% NaCl and reported an increased oxide film formation with an increase in exposure duration up to 25 days. The results obtained from OCP measurements were correlated with polarization resistance measurements and were found to follow the same trend. Saker et al. [34] reported the inhibition of carbon steel corrosion in 3% NaCl using OCP measurements. The potential of carbon steel was shifted toward more negative values in the first few minutes of immersion due to chloride attack
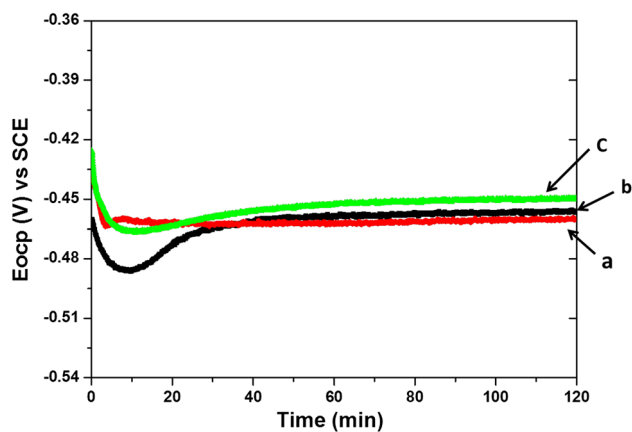
Fig. 1 Open-circuit potential (E_{ocp}) versus time curves of mild steel in 1.0 M HCl in the absence: **a** blank; and in the presence of: 50 ppm **b** 2-EM-Imz and **c** 1-B-Imz at 500 rpm electrode rotation, bottom to top

and later to less negative values due to the formation of relatively stable oxide films. The formation of a self-assembled layer of phosphono molecules on iron was studied by Felhosi et al. [35]. A corresponding shift of E_{corr} in the anodic direction was observed and attributed to the adsorption of the phosphono compounds on the surface of iron. In general, OCP measurements can provide information whether the system under investigation is in the active or passive state. OCP measurement data can serve as a starting point in evaluating the electrochemical performance of different materials with/without the presence of inhibitors.

3.3 Hydrodynamic Studies

3.3.1 Tafel Polarization Measurements

Tafel polarization experiments to evaluate the corrosion performance of API X65 steel were carried out in 1.0 M HCl solution with and without inhibitor molecules under both static and dynamic conditions. Preliminary studies showed an increase in the corrosion rate of API X65 steel with an increase in rotation rate when compared with its behavior under static condition. This trend was also observed when 50 ppm of inhibitor molecules was added to the medium. Electrochemical data obtained from Tafel polarization in terms of corrosion potential (E_{corr}), anodic and cathodic Tafel slopes (β_a and β_c), corrosion current density (i_{corr}) and corrosion rate are presented in Table 4. The inhibition efficiencies (%Inh) were calculated using the equation:

$$\%\text{Inh} = \left(\frac{i_{corr}^{\circ} - i_{corr}}{i_{corr}^{\circ}} \right) \times 100 \tag{6}$$

where i_{corr}^o and i_{corr} are corrosion current densities in the absence and presence of inhibitor molecules, respectively [36].

Organic molecules containing heteroatoms such as N and O are considered a class of inhibitor molecules that tend to adsorb on steel through donor–acceptor interaction mechanism to form a protective barrier which prevents the metal from undergoing corrosion [37]. It is generally believed that the first step in the adsorption of such molecules on a metal is the displacement of one or more molecules of water on the surface which is then followed by the combination of a freshly generated Fe^{2+} ions on the steel surface to form metal–inhibitor complex [38]. The complex formed depending on its solubility can either lead to more metal dissolution or inhibit further dissolution. In most cases, the complex formed shield water molecules from reaching the metal, thereby forcing iron into passivation [38]. Usually in acidic medium, the inhibition effect can be due to metal ion inhibitor complexation or more likely as a result of physisorption.

Hydrodynamic conditions affect the corrosion inhibition of organic molecules and this is mainly because under flow conditions, several factors play a role on the inhibitive performance of such molecules [39] such as:

I. Mass transport of the inhibitor molecules can increase under flow conditions causing more inhibitor molecules to be present at metal surface. If this happens, the inhibitive performance of the molecule is observed with increasing flow.

II. Mass transport of metal ions produced during dissolution can increase under flow conditions from the metal surface to the bulk of the solution. If this happens, less metal–inhibitor complex will be present at the metal surface. Hence, the metal dissolution will be enhanced.

III. The high shear stress resulting from high flow velocity in turbulent flows can lead to the detachment of adsorbed inhibitor molecules from the metal surface exposing the metal to the aggressive medium and that will lead to more dissolution of the metal

To check the flow of the system whether it follows the laminar or turbulent flow principle, Reynolds number (Re) was calculated using the equation:

$$Re = \frac{r^2 \omega}{k_v} \tag{7}$$

where r is the radius of the RDE active area in mm, ω the angular velocity in rad/s and k_v the kinematic viscosity of the medium in stokes (mm^2/s), respectively [38]. The Reynolds number is used for predicting whether a flow condition will be turbulent or laminar. Lower values of Re (less than 2000) indicate that fluid particles move in straight line

Table 4 Electrochemical data derived from Tafel at 50 ppm inhibitor molecules

Rotation speed (rpm)	Reynolds number	E_{corr}/V versus SCE	β_a (V/dec)	$-\beta_c$ (V/dec)	$I_{corr}(x10^{-4})$/A cm^{-2}	Corrosion rate (mpy)	% Inh.
1.0M HCl							
0	0	-0.522	0.074	0.122	2.29	104.3	–
500	600	-0.466	0.078	0.192	2.62	124.2	–
1000	1200	-0.452	0.056	0.143	3.48	158.6	–
1500	1800	-0.455	0.066	0.284	4.63	211.0	–
2-EM-Imz							
0	0	-0.528	0.074	0.082	1.21	55.06	47.2
500	600	-0.469	0.042	0.229	2.09	99.08	20.2
1000	1200	-0.483	0.065	0.132	3.04	138.55	12.6
1500	1800	-0.487	0.097	0.230	6.36	289.40	–
1-B-Imz							
0	0	-0.516	0.079	0.123	1.21	55.26	47.2
500	600	-0.481	0.069	0.167	2.02	95.76	22.9
1000	1200	-0.484	0.070	0.131	3.16	144.00	9.2
1500	1800	-0.460	0.069	0.196	4.49	204.70	3.0

flowing over one another at different speeds with virtually no mixing between the layers; hence, the flow is said to be laminar. Larger values of *Re* (greater than 8000) on the other hand imply that the flow is characterized by irregular movement of particles of the fluid with high velocity, and such flow is said to be turbulent [38]. The values of *Re* obtained in this study as shown in Table 4 indicates that the flow of the medium follows the laminar principle; hence, other factors already highlighted could account for the observed increase in corrosion current as shown in Table 4.

The observed increase in corrosion current with an increase in electrode rotation (0–1500 rpm) with a consequent decrease in the inhibitive performance of the molecules under study is attributed to the increase in mass transport of the metal ions from the metal surface to the bulk of solution leading to less surface coverage by the inhibitor molecules. Hence, to further study the effect of the inhibitor molecules on the corrosion of API X65 steel under dynamic conditions, Tafel polarization measurements were further taken by increasing the concentration of the inhibitor molecules (50–500 ppm) at 500 rpm electrode rotation in order to observe whether mass transport of the inhibitor molecules to the metal surface will overcome that of the metal ions into the bulk of solution as shown in Fig. 2.

It was found that increasing the concentrations of the inhibitor molecules under dynamic conditions tends to reduce the dissolution of the metal ions. This reduction was attributed to the mass transport of the inhibitor molecules to the metal surface as more molecules are now present in the medium. The observed reduction was, however, more pronounced in the case of 1-B-Imz which was found to have an

inhibition efficiency of 82% due to the presence of an aromatic ring in the molecule. It has been proposed that among the mechanisms by which organic molecules adsorb on a metal is through π–electron interactions between the aromatic rings (if present) in the molecules and Fe^{2+} of the metal forming Fe–Inh complex [37]. It is this complex that forms the protective film on the metal which tends to prevent it from further dissolution. The electrochemical data extracted from the Tafel polarization curves are given in Table 5.

Tafel polarization method is a very reliable tool to study the corrosion process as it provides information such as corrosion potential, corrosion current density and corrosion rate of the material under investigation. McCafferty [40] reported the validation of corrosion rates measured by Tafel extrapolation in the corrosion of metals such as iron and titanium using non-electrochemical methods in HCl, 3.5% NaCl and H_2SO_4. A good agreement was found between the rates found from Tafel extrapolation and the non-electrochemical methods. Shi et al. [41] evaluated the reliability of corrosion rate measurements of magnesium alloys by Tafel extrapolation method and reported that, unlike iron, aluminum and copper alloys, results obtained for magnesium alloys did not agree with those from weight loss and hydrogen evolution measurements. Marco et al. [42] later confirmed that corrosion parameters of the electrochemical corrosion of magnesium obtained from Tafel extrapolation could be reliable under dynamic conditions. This study confirms the reliability of Tafel extrapolation methods for determining corrosion rate of iron under dynamic conditions as the results obtained were not significantly different from those obtained using AC impedance technique.
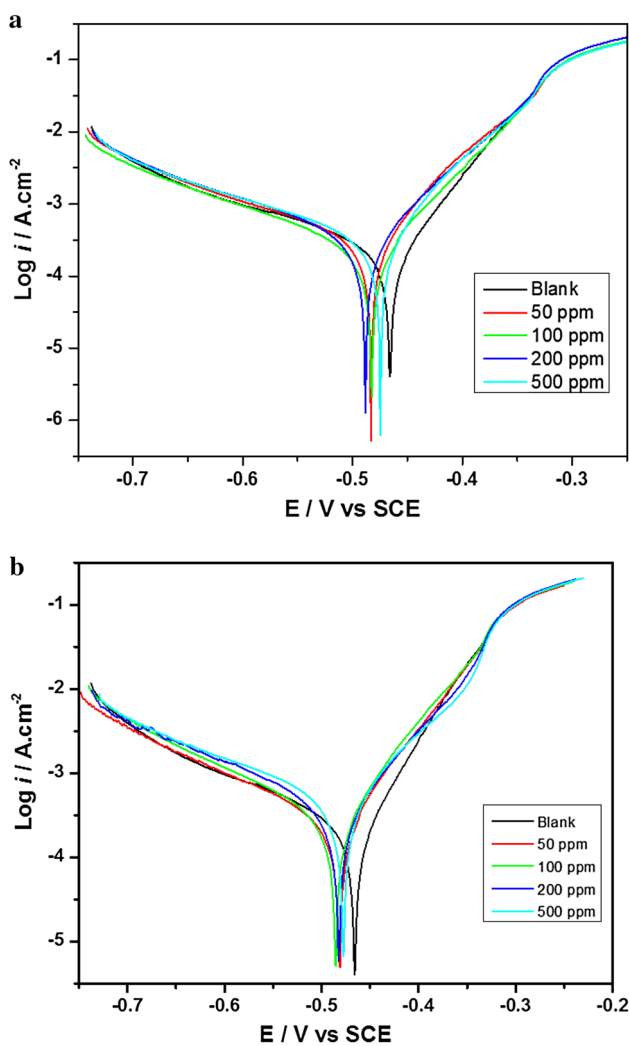
Fig. 2 Tafel polarization curves for corrosion of mild steel at 500 rpm electrode rotation and 50–500 ppm: **a** 2-EM-Imz and **b** 1-B-Imz

3.3.2 Electrochemical Impedance Spectroscopy (EIS) Measurements

EIS is a useful technique in corrosion and other surface and electrochemical studies. In this technique, a small amplitude sinusoidal perturbation is applied to the steel specimen and the resulting impedance is measured; hence, it is regarded as a less intrusive technique. It is capable of revealing the mechanism of film formation on the surface of the metal and the persistence or otherwise of such films. It also yields information such as interfacial properties of a metal where basic microscopic reactions take place, and from these properties, electrochemical features of an electrically conducting surface are extracted [43–45].

EIS measurements were taken under dynamic conditions in the presence of the inhibitors under study by varying the concentration of the inhibitor molecules. Inhibition efficiencies were calculated using the equation:

$$\eta\,(\%) = \left(\frac{R_{ct} - R_{ct}^{\circ}}{R_{ct}} \right) \times 100 \tag{8}$$

where R_{ct} and R_{ct}^{o} are the charge transfer resistances of the metal in the presence and absence of the inhibitor molecules, respectively [46]. Figure 3 shows the Nyquist plots of the two inhibitor molecules obtained by varying their concentrations (50–500 ppm) and under hydrodynamic conditions.

The Nyquist plots in both cases give a depressed semi-circle, an indication that there is only one time constant equivalent to the charge transfer process in the system [47]. In addition, the observed depressed capacitive loops are as a result of the dispersion effect which occurs due to the roughness of the metal surface, existence of porous layers on the surface and adsorption of the inhibitor molecules onto the surface [48]. The addition of the inhibitors resulted into an increase in the capacitive loop diameter compared to the uninhibited medium, and this increased as the concentration of the inhibitors was increased due to an increase in surface coverage (θ) of the molecules. The charge transfer resis-

Table 5 Electrochemical data derived from Tafel measurements at 50–500 ppm inhibitor

| Medium	Inhibitor conc. (ppm)	E_{corr}/V versus SCE	β_a (V/dec)	$-\beta_c$ (V/dec)	$I_{corr}(\times 10^{-4})$/A cm^{-2}	Corrosion rate (mpy)	% Inh.
Blank	0	− 0.466	0.078	0.192	2.62	124.2	–
2-EM-Imz	50	− 0.469	0.042	0.229	2.09	99.08	20.2
	100	− 0.483	0.066	0.131	1.89	86.05	30.9
	200	− 0.488	0.047	0.071	1.25	59.26	52.3
	500	− 0.475	0.041	0.072	0.65	30.81	75.2
1-B-Imz	50	− 0.481	0.069	0.167	2.02	95.8	22.9
	100	− 0.485	0.064	0.128	1.78	84.4	32.1
	200	− 0.482	0.079	0.154	1.06	50.3	59.5
	500	− 0.478	0.075	0.151	0.47	22.2	82.1
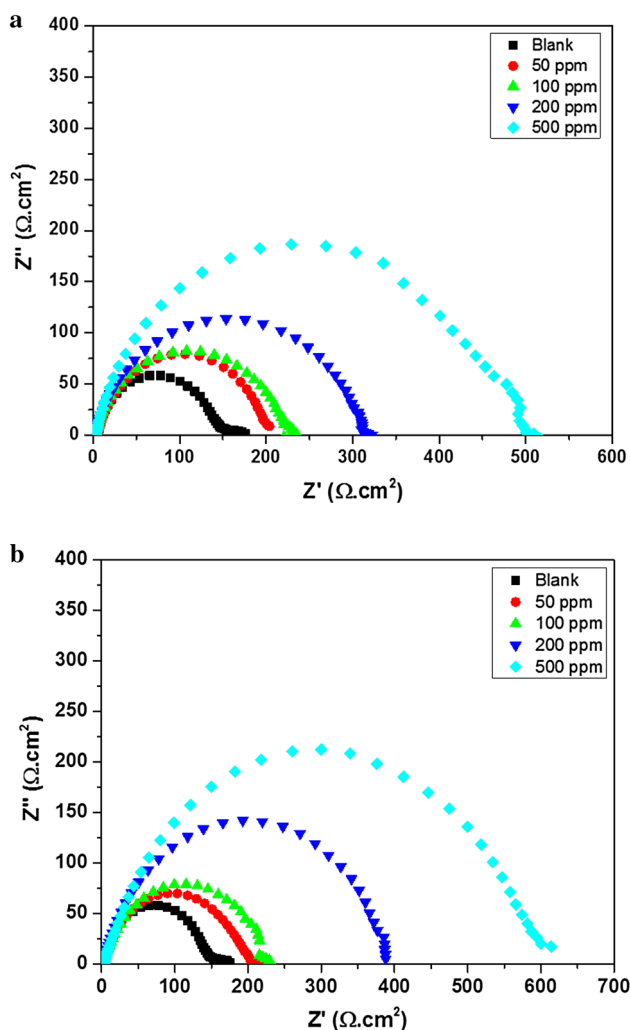
Fig. 3 Nyquist plots for corrosion of mild steel at 500 rpm electrode rotation and 50–500 ppm: **a** 2-EM-Imz and **b** 1-B-Imz

tance which is the resistance to the flow of electrons in the corrosion of the metal significantly increases upon addition of the inhibitor molecules compared to the uninhibited solution. This is attributed to the mass transport of the inhibitor

molecules to the electrode, thereby reducing the rate of dissolution of the metal as was evidenced by the continuous increase in the Rct values with increasing inhibitor concentrations [49]. The results of the EIS measurements are given in Table 6.

The equivalent circuit utilized in the extraction of EIS data and representatives of the fitted Nyquist curve are shown in Fig. 4a–c. It consists of a parallel arrangement of charge transfer resistance (R_{ct}) which is the resistance due to electron transfer across the specimen and a constant phase element (CPE), both in series with the solution resistance (R_s). The constant phase element was included in the model in order to account for the local inhomogeneity in the dielectric material and the porosity in mass transport effects [50].

The impedance of constant phase element is given as:

$$Z_{CPE} = \frac{1}{Q\,(i\omega)^n} \tag{9}$$

where Q is the magnitude of CPE, n the phase shift, ω the angular frequency and i an imaginary number. The interpretation of CPE is determined by the value of n, where $n = 0$ implies that CPE represents a resistance, $n = 1$ a capacitance and $n = -1$, an inductance.

The double-layer capacitance C_{dl} is estimated using the equation:

$$C_{dl} = \frac{1}{2\pi\,f_{max}\,R_{ct}} \tag{10}$$

where f_{max} stands for maximum frequency of the imaginary component of the impedance and Rct the charge transfer resistance.

From the results presented in Table 6, there was a significant decrease in C_{dl} upon addition of the inhibitor molecules which is due to an increase in the double-layer thickness resulting from the adsorption of the inhibitors. This is in agreement with the mathematical expression of the Helmholtz model [51] given as:

Table 6 Electrochemical data derived from EIS measurements at 50–500 ppm inhibitors

Medium	Inhibitor conc. (ppm)	R_s ($\Omega\,cm^2$)	R_{ct} ($\Omega\,cm^2$)	C_{dl} ($\mu F\,cm^{-2}$)	n	θ	% Inh.
Blank	0	4.384	147.5	215.4	0.88	–	–
2-EM-Imz	50	2.535	197.2	22.64	0.86	0.25	25.2
	100	2.718	222.0	22.04	0.84	0.34	33.6
	200	2.466	308.8	25.95	0.83	0.52	52.2
	500	2.601	488.5	16.41	0.84	0.70	70.0
1-B-Imz	50	2.519	196.7	20.37	0.83	0.25	25.0
	100	2.377	224.0	28.50	0.80	0.34	34.2
	200	2.708	385.0	20.82	0.81	0.62	61.7
	500	2.772	610.2	26.27	0.80	0.76	76.0

Fig. 4 **a** EIS model used to fit the Nyquist data obtained in figure. Curve fitting to Nyquist data of mild steel at 500 rpm electrode rotation and 50–500 in: **b** 2-EM-Imz and **c** 1-B-Imz
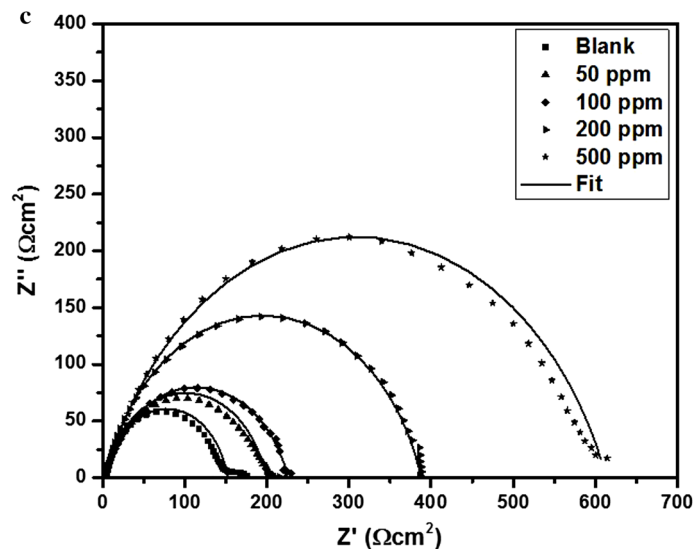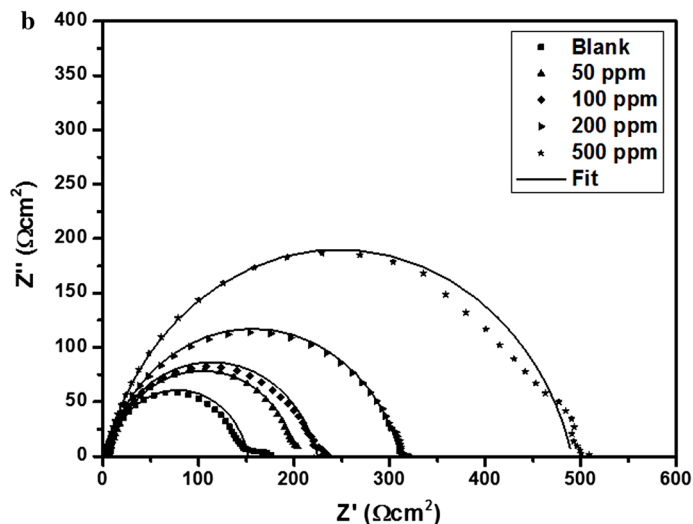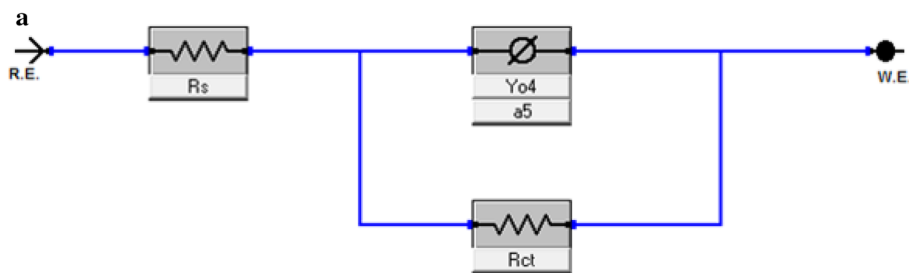
$$C_{dl} = \frac{\varepsilon \varepsilon_o A}{d} \tag{11}$$

where d is the thickness of the protective layer, ε the dielectric constant, ε_o vacuum permittivity and A the effective surface area of electrode. 1-B-Imz was found to have a surface coverage of 0.76 and a dynamic corrosion inhibition of 76% at 500 ppm. This is attributed to the presence of delocalized pi electrons in its molecular backbone which tends to form a stronger adsorption.

3.4 Adsorption Isotherms

One important feature of organic corrosion inhibitors is their ability to adsorb on metallic surfaces forming a protective film. Adsorption is a surface phenomenon and a consequence of surface energy. Solids are usually in a state of strain which leads to unbalanced residual forces on their surfaces. These forces cause solids to have high surface energies, and hence, they have the tendency to attract and retain molecu-

lar species with which they come in contact, a phenomenon known as adsorption. Adsorption could be through electrostatic attractions between charged molecules and the metal ions or through electron transfer and/or sharing between the molecules and the metal ions. The former is known as physisorption, while the latter is known as chemisorption.

In corrosion inhibition studies, adsorption isotherms are used to propose the mechanism through which inhibitor molecules interacts with the metal ions [46], by first determining the extent of surface coverage θ of the molecules. Surface coverage is a dimensionless parameter derived from the charge transfer resistances of the inhibitor molecules using the equation:

$$\theta = \left(\frac{R_{ct} - R_{ct}^{\circ}}{R_{ct}} \right) \tag{12}$$

as already presented in Table 6.

Langmuir, Temkin and Frumkin isotherms are among the commonly used models each of which relates the surface coverage of a given adsorbate to its concentration [52]. Langmuir model proposes that an adsorbate only covers one substrate site, that surface free energy of all sites on the substrate is equal and that no interaction occurs between the adsorbed species. However, once the concentration of the adsorbed species is high to the extent that there is the possibility of attractive or repulsive interactions among the species, this model fails and it becomes necessary to fit using either the Frumkin or Temkin isotherms.

The results obtained in this study were fitted into the three adsorption models and were found to fit well into the Langmuir adsorption model which is represented as follows:

$$\frac{C}{\theta} = \frac{1}{K_{ads}} + C \tag{13}$$

where K_{ads} is the adsorption equilibrium constant. The Gibbs free energy of adsorption was calculated by the equation:

$$\Delta G_{ads} = -RT \ln (55.5 K_{ads}) \tag{14}$$

where R is the molar gas constant, T the absolute temperature and 55.5 the molar concentration of water [52]. The plot of Langmuir adsorption isotherm of the inhibitor molecules under study is shown in Fig. 5, while the corresponding adsorption parameters are given in Table 7.

Typical values of ΔG_{ads} up to around -20 KJ are usually ascribed to electrostatic interactions (physisorption), while values around -40 KJ or higher are associated with electron transfer or sharing between the adsorbate and the substrate (metal ions) to form a coordinate type of bond (chemisorption) [27]. The values obtained in this study fall between the two which shows a mixture of physical and chemical interactions between the inhibitor molecules and the metal ions.
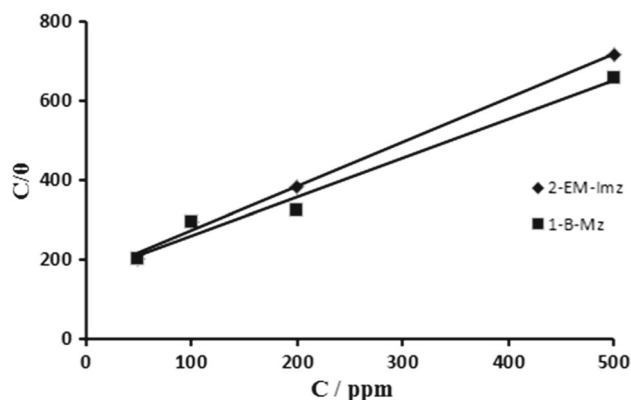

Fig. 5 Langmuir adsorption isotherm plots of the studied inhibitor molecules

Table 7 Adsorption parameters for 2-I-Imz and 2-Cl-Imz

Inhibitor	$K_{ads}(x10^3 Lmol^{-1})$	$\Delta G_{ads}(KJmol^{-1})$	R^2
2-EM-Imz	0.676	-26.10	0.995
1-B-Imz	0.687	-26.14	0.980

4 Conclusions

The corrosion inhibitive performance of two imidazole molecules under hydrodynamic conditions was successfully carried out. DFT calculations conducted at B3LYP/6-31G(d.p) on the molecules predicted 1-benzylimidazole as a better corrosion inhibitor due to its low energy gap and low global hardness in aqueous medium. The inhibitor molecules were found to decrease the rate of dissolution of iron due to mass transport to the surface of the metal under dynamic conditions with an overall inhibition efficiency of 82% achieved in 1-benzylimidazole at 500 ppm and 500 rpm electrode rotation. Adsorption studies carried out showed a mixture of physical and chemical interactions between the molecules and the metal and were found to fit the Langmuir adsorption isotherm. Overall, the study demonstrates that simple imidazole molecules could serve as corrosion inhibitors under extreme hydrodynamic conditions primarily due to their kinetic control and strong adsorption on the surface.

References

1. Cruz, J.; Martınez, R.; Genesca, J.; Garcıa-Ochoa, E.: Experimental and theoretical study of 1-(2-ethylamino)-2-methylimidazoline as an inhibitor of carbon steel corrosion in acid media. J. Electroanal. Chem. **566**(1), 111–121 (2004)

2. Rauscher, A.; Kutsan, G.; Lukacs, Z.: Studies on the mechanisms of corrosion inhibition by acetylenic compounds in hydrochloric acid solution. Corros. Sci. **35**(5–8), 1425–1430 (1993)

3. Wang, D.; Li, S.; Ying, Y.; Wang, M.; Xiao, H.; Chen, Z.: Theoretical and experimental studies of structure and inhibition efficiency of imidazoline derivatives. Corro. Sci. **41**(10), 1911–1919 (1999)

4. Xia, S.; Qiu, M.; Yu, L.; Liu, F.; Zhao, H.: Molecular dynamics and density functional theory study on relationship between structure of imidazoline derivatives and inhibition performance. Corro. Sci. **50**(7), 2021–2029 (2008). https://doi.org/10.1016/j.corsci.2008.04.021

5. Bommersbach, P.; Alemany-Dumont, C.; Millet, J.-P.; Normand, B.: Hydrodynamic effect on the behaviour of a corrosion inhibitor film: characterization by electrochemical impedance spectroscopy. Electrochim. Acta **51**(19), 4011–4018 (2006)

6. Bommersbach, P.; Alemany-Dumont, C.; Millet, J.-P.; Normand, B.: Formation and behaviour study of an environment-friendly corrosion inhibitor by electrochemical methods. Electrochim. Acta **51**(6), 1076–1084 (2005)

7. Braga, D.U.; Diniz, A.E.; Miranda, G.W.; Coppini, N.L.: Using a minimum quantity of lubricant (MQL) and a diamond coated tool in the drilling of aluminum-silicon alloys. J. Mater. Process. Technol. **122**(1), 127–138 (2002)

8. Mansfeld, F.; Kendig, M.; Lorenz, W.: Corrosion inhibition in neutral, aerated media. J. Electrochem. Soc. **132**(2), 290–296 (1985)

9. Bahrami, M.; Hosseini, S.; Pilvar, P.: Experimental and theoretical investigation of organic compounds as inhibitors for mild steel corrosion in sulfuric acid medium. Corros. Sci. **52**(9), 2793–2803 (2010)

10. Zhang, Q.; Hua, Y.: Corrosion inhibition of mild steel by alkylimidazolium ionic liquids in hydrochloric acid. Electrochim. Acta **54**(6), 1881–1887 (2009)

11. Zhang, F.; Tang, Y.; Cao, Z.; Jing, W.; Wu, Z.; Chen, Y.: Performance and theoretical study on corrosion inhibition of 2-(4-pyridyl)-benzimidazole for mild steel in hydrochloric acid. Corros. Sci. **61**, 1–9 (2012)

12. Obot, I.; Umoren, S.; Gasem, Z.; Suleiman, R.; El Ali, B.: Theoretical prediction and electrochemical evaluation of vinylimidazole and allylimidazole as corrosion inhibitors for mild steel in 1 M HCl. J. Ind. Eng. Chem. **21**, 1328–1339 (2015)

13. Morales-Gil, P.; Walczak, M.; Cottis, R.; Romero, J.; Lindsay, R.: Corrosion inhibitor binding in an acidic medium: interaction of 2-mercaptobenizmidazole with carbon-steel in hydrochloric acid. Corros. Sci. **85**, 109–114 (2014)

14. Khaled, K.; Amin, M.A.: Electrochemical and molecular dynamics simulation studies on the corrosion inhibition of aluminum in molar hydrochloric acid using some imidazole derivatives. J. Appl. Electrochem. **39**(12), 2553–2568 (2009)

15. Şahin, M.; Bilgic, S.; Yılmaz, H.: The inhibition effects of some cyclic nitrogen compounds on the corrosion of the steel in NaCl mediums. Appl. Surf. Sci. **195**(1), 1–7 (2002)

16. Gece, G.; Bilgiç, S.: Quantum chemical study of some cyclic nitrogen compounds as corrosion inhibitors of steel in NaCl media. Corros. Sci. **51**(8), 1876–1878 (2009)

17. Cruz, J.; Garcia-Ochoa, E.; Castro, M.: Experimental and theoretical study of the 3-amino-1,2,4-triazole and 2-aminothiazole corrosion inhibitors in carbon steel. J. Electrochem. Soc. **150**(1), B26–B35 (2003)

18. Cruz, J.; Pandiyan, T.; Garcia-Ochoa, E.: A new inhibitor for mild carbon steel: electrochemical and DFT studies. J. Electroanal. Chem. **583**(1), 8–16 (2005)

19. Nikolic, J.; Expósito, E.; Iniesta, J.; González-García, J.; Montiel, V.: Theoretical concepts and applications of a rotating disk electrode. J. Chem. Educ. **77**(9), 1191 (2000)

20. Liu, G.; Tree, D.; High, M.: Relationships between rotating disk corrosion measurements and corrosion in pipe flow. Corrosion **50**(8), 584–593 (1994)

21. Taylor, K.; Nasr-El-Din, H.: Measurement of acid reaction rates with the rotating disk apparatus. J. Can. Pet. Technol. **48**(06), 66–70 (2009)

22. Becerra, H.Q.; Retamoso, C.; Macdonald, D.D.: The corrosion of carbon steel in oil-in-water emulsions under controlled hydrodynamic conditions. Corros. Sci. **42**(3), 561–575 (2000)

23. Dinan, T.; Matlosz, M.; Landolt, D.: Experimental investigation of the current distribution on a recessed rotating disk electrode. J. Electrochem. Soc. **138**(10), 2947–2951 (1991)

24. Frisch, M.J.; Trucks, G.W.; Schlegel, H.B.; Scuseria, G.E.; Robb, M.A.; Cheeseman, J.R.; Scalmani, G.; Barone, V.; Mennucci, B.; Petersson, G.A.; Nakatsuji, H.; Caricato, M.; Li, X.; Hratchian, H.P.; Izmaylov, A.F.; Bloino, J.; Zheng, G.; Sonnenberg, J.L.; Hada, M.; Ehara, M.; Toyota, K.; Fukuda, R.; Hasegawa, J.; Ishida, M.; Nakajima, T.; Honda, Y.; Kitao, O.; Nakai, H.; Vreven, T.; Montgomery, J.A.; Peralta, J.E.; Ogliaro, F.; Bearpark, M.; Heyd, J.J.; Brothers, E.; Kudin, K.N.; Staroverov, V.N.; Kobayashi, R.; Normand, J.; Raghavachari, K.; Rendell, A.; Burant, J.C.; Iyengar, S.S.; Tomasi, J.; Cossi, M.; Rega, N.; Millam, J.M.; Klene, M.; Knox, J.E.; Cross, J.B.; Bakken, V.; Adamo, C.; Jaramillo, J.; Gomperts, R.; Stratmann, R.E.; Yazyev, O.; Austin, A.J.; Cammi, R.; Pomelli, C.; Ochterski, J.W.; Martin, R.L.; Morokuma, K.; Zakrzewski, V.G.; Voth, G.A.; Salvador, P.; Dannenberg, J.J.; Dapprich, S.; Daniels, A.D.; Farkas Foresman, J.B.; Ortiz, J.V.; Cioslowski, J.; Fox, D.J.: Gaussian 09, Revision B.01. Gaussian, Inc., Wallingford CT (2009)

25. Sulaiman, K.O.; Onawole, A.T.: Quantum chemical evaluation of the corrosion inhibition of novel aromatic hydrazide derivatives on mild steel in hydrochloric acid. Comput. Theor. Chem. **1093**, 73–80 (2016). https://doi.org/10.1016/j.comptc.2016.08.014

26. Khaled, K.F.: Studies of iron corrosion inhibition using chemical, electrochemical and computer simulation techniques. Electrochim. Acta **55**(22), 6523–6532 (2010). https://doi.org/10.1016/j.electacta.2010.06.027

27. Obot, I.B.; Obi-Egbedi, N.O.: Theoretical study of benzimidazole and its derivatives and their potential activity as corrosion inhibitors. Corros. Sci. **52**(2), 657–660 (2010). https://doi.org/10.1016/j.corsci.2009.10.017

28. Mendonça, G.L.F.; Costa, S.N.; Freire, V.N.; Casciano, P.N.S.; Correia, A.N.; Lima-Neto, Pd: Understanding the corrosion inhibition of carbon steel and copper in sulphuric acid medium by amino acids using electrochemical techniques allied to molecular modelling methods. Corros. Sci. **115**, 41–55 (2017). https://doi.org/10.1016/j.corsci.2016.11.012

29. Feng, L.; Yang, H.; Wang, F.: Experimental and theoretical studies for corrosion inhibition of carbon steel by imidazoline derivative in 5% NaCl saturated Ca(OH)$_2$ solution. Electrochim. Acta **58**, 427–436 (2011). https://doi.org/10.1016/j.electacta.2011.09.063

30. Yadav, M.; Kumar, S.; Purkait, T.; Olasunkanmi, L.O.; Bahadur, I.; Ebenso, E.E.: Electrochemical, thermodynamic and quantum chemical studies of synthesized benzimidazole derivatives as corrosion inhibitors for N80 steel in hydrochloric acid. J. Mol. Liq. **213**, 122–138 (2016). https://doi.org/10.1016/j.molliq.2015.11.018

31. Kumar, S.; Vashisht, H.; Olasunkanmi, L.O.; Bahadur, I.; Verma, H.; Singh, G.; Obot, I.B.; Ebenso, E.E.: Experimental and theoretical studies on inhibition of mild steel corrosion by some synthesized polyurethane tri-block co-polymers. Sci. Rep. **6**, 30937 (2016). https://doi.org/10.1038/srep30937

32. Chattaraj, P.K.; Lee, H.; Parr, R.G.: HSAB principle. J. Am. Chem. Soc. **113**(5), 1855–1856 (1991). https://doi.org/10.1021/ja00005a073

33. Choudhary, S.; Garg, A.; Mondal, K.: Relation between open circuit potential and polarization resistance with rust and corrosion

monitoring of mild steel. J. Mat. Eng. Perform. **25**(7), 2969–2976 (2016). https://doi.org/10.1007/s11665-016-2112-6

34. Saker, S.; Aliouane, N.; Hammache, H.; Chafaa, S.; Bouet, G.: Tetraphosphonic acid as eco-friendly corrosion inhibitor on carbon steel in 3 % NaCl aqueous solution. Ionics **21**(7), 2079–2090 (2015). https://doi.org/10.1007/s11581-015-1377-3

35. Felhösi, I.; Telegdi, J.; Pálinkás, G.; Kálmán, E.: Kinetics of self-assembled layer formation on iron. Electrochim. Acta **47**(13), 2335–2340 (2002). https://doi.org/10.1016/S0013-4686(02)00084-1

36. Yıldırım, A.; Çetin, M.: Synthesis and evaluation of new long alkyl side chain acetamide, isoxazolidine and isoxazoline derivatives as corrosion inhibitors. Corros. Sci. **50**(1), 155–165 (2008). https://doi.org/10.1016/j.corsci.2007.06.015

37. Zeino, A.; Abdulazeez, I.; Khaled, M.; Jawich, M.W.; Obot, I.B.: Mechanistic study of polyaspartic acid (PASP) as eco-friendly corrosion inhibitor on mild steel in 3% NaCl aerated solution. J. Mol. Liq. **250**, 50–62 (2018). https://doi.org/10.1016/j.molliq.2017.11.160

38. Ashassi-Sorkhabi, H.; Asghari, E.: Effect of hydrodynamic conditions on the inhibition performance of l-methionine as a "green" inhibitor. Electrochim. Acta **54**(2), 162–167 (2008). https://doi.org/10.1016/j.electacta.2008.08.024

39. Jiang, X.; Zheng, Y.G.; Ke, W.: Effect of flow velocity and entrained sand on inhibition performances of two inhibitors for CO$_2$ corrosion of N80 steel in 3% NaCl solution. Corros. Sci. **47**(11), 2636–2658 (2005). https://doi.org/10.1016/j.corsci.2004.11.012

40. McCafferty, E.: Validation of corrosion rates measured by the Tafel extrapolation method. Corros. Sci. **47**(12), 3202–3215 (2005). https://doi.org/10.1016/j.corsci.2005.05.046

41. Shi, Z.; Liu, M.; Atrens, A.: Measurement of the corrosion rate of magnesium alloys using Tafel extrapolation. Corros. Sci. **52**(2), 579–588 (2010). https://doi.org/10.1016/j.corsci.2009.10.016

42. Marco, I.; Van der Biest, O.: Polarization measurements from a rotating disc electrode for characterization of magnesium corrosion. Corros. Sci. **102**, 384–393 (2016). https://doi.org/10.1016/j.corsci.2015.10.031

43. Garcia, L.A.C.J.; Joia, C.J.B.M.; Cardoso, E.M.; Mattos, O.R.: Electrochemical methods in corrosion on petroleum industry: laboratory and field results. Electrochim. Acta **46**(24–25), 3879–3886 (2001). https://doi.org/10.1016/S0013-4686(01)00675-2

44. Wang, Z.; Li, J.; Wang, Y.; Wang, Z.: An EIS analysis on corrosion resistance of anti-abrasion coating. Surf. Interfaces **6**, 33–39 (2017). https://doi.org/10.1016/j.surfin.2016.11.003

45. Ribeiro, D.V.; Abrantes, J.C.C.: Application of electrochemical impedance spectroscopy (EIS) to monitor the corrosion of reinforced concrete: a new approach. Constr. Build. Mater. **111**, 98–104 (2016). https://doi.org/10.1016/j.conbuildmat.2016.02.047

46. Gutiérrez, E.; Rodríguez, J.A.; Cruz-Borbolla, J.; Alvarado-Rodríguez, J.G.; Thangarasu, P.: Development of a predictive model for corrosion inhibition of carbon steel by imidazole and benzimidazole derivatives. Corros. Sci. **108**, 23–35 (2016). https://doi.org/10.1016/j.corsci.2016.02.036

47. Aljourani, J.; Raeissi, K.; Golozar, M.A.: Benzimidazole and its derivatives as corrosion inhibitors for mild steel in 1 M HCl solution. Corros. Sci. **51**(8), 1836–1843 (2009). https://doi.org/10.1016/j.corsci.2009.05.011

48. Solmaz, R.; Kardaş, G.; Çulha, M.; Yazıcı, B.; Erbil, M.: Investigation of adsorption and inhibitive effect of 2-mercaptothiazoline on corrosion of mild steel in hydrochloric acid media. Electrochim. Acta **53**(20), 5941–5952 (2008). https://doi.org/10.1016/j.electacta.2008.03.055

49. Coelho, L.B.; Cossement, D.; Olivier, M.G.: Benzotriazole and cerium chloride as corrosion inhibitors for AA2024-T3: an EIS investigation supported by SVET and ToF-SIMS analysis. Corros. Sci. **130**, 177–189 (2018). https://doi.org/10.1016/j.corsci.2017.11.004

50. Odewunmi, N.A.; Umoren, S.A.; Gasem, Z.M.: Utilization of watermelon rind extract as a green corrosion inhibitor for mild steel in acidic media. J. Ind. Eng. Chem. **21**, 239–247 (2015). https://doi.org/10.1016/j.jiec.2014.02.030

51. Khaled, K.F.; Al-Qahtani, M.M.: The inhibitive effect of some tetrazole derivatives towards Al corrosion in acid solution: chemical, electrochemical and theoretical studies. Mater. Chem. Phys. **113**(1), 150–158 (2009). https://doi.org/10.1016/j.matchemphys.2008.07.060

52. Daoud, D.; Douadi, T.; Hamani, H.; Chafaa, S.; Al-Noaimi, M.: Corrosion inhibition of mild steel by two new S-heterocyclic compounds in 1 M HCl: Experimental and computational study. Corros. Sci. **94**, 21–37 (2015). https://doi.org/10.1016/j.corsci.2015.01.025